

Spatially Controlled Lithium Deposition on Silver-Nanocrystals-Decorated TiO₂ Nanotube Arrays Enabling Ultrastable Lithium Metal Anode

Yanzhong Lu, Jinshan Wang, Yang Chen, Xinyu Zheng, Hurong Yao, Sanjay Mathur, and Zhensheng Hong*

3D scaffolds and heterogeneous seeds are two effective ways to guide Li deposition and suppress Li dendrite growth. Herein, 3D TiO₂ nanotube (TNT) arrays decorated using ultrafine silver nanocrystals (7–10 nm) through cathodic reduction deposition are first demonstrated as a confined space host for lithium metal deposition. First, TiO₂ possesses intrinsic lithium affinity with large Li absorption energy, which facilitates Li capture. Then, ultrafine silver nanocrystals decoration allows the uniform and selective nucleation in nanoscale without a nucleation barrier, leading to the extraordinary formation of lithium metal importing into 3D nanotube arrays. As a result, Li metal anode deposited on such a binary architecture (TNT-Ag-Li) delivers a high Coulomb efficiency at around 99.4% even after 300 cycles with a capacity of 2 mA h cm⁻². Remarkably, TNT-Ag-Li exhibits ultralow overpotential of 4 mV and long-term cycling life over 2500 h with a capacity of 2 mAh cm⁻² in Li symmetric cells. Moreover, the full battery with 3D spaced Li nanotubes anode and LiFeO₄ cathode exhibits a stable and high capacity of 115 mA h g⁻¹ at 5 C and an excellent Coulombic efficiency of ≈100% over 500 cycles.

the increasing needs, so the next-generation batteries with energy density over 500 W h kg⁻¹ have become one of the hot spots and focuses of current research.^[2,3] Lithium metal anode, with ultrahigh theoretical capacity (3860 mAh g⁻¹) and lowest working potential, is regarded as an ideal anode for Li-S, Li-O₂ batteries or other intercalation type cathode batteries enabling high-energy-density Li metal batteries (LMBs).^[4–6] However, such battery technology suffers from poor cycling stability and safety concerns from the side of Li anode. The uncontrollability of lithium dendrites, the accumulation of dead lithium inside the too thick SEI film arising from the serious electrolytes decomposition with highly active lithium, and large volume change during lithium plating and stripping seriously hinders its practical development.^[7–11]

1. Introduction

The fast development of electric vehicles and hybrid electric vehicles has pushed explosive demand for high energy density batteries.^[1] The energy density of current lithium ion batteries (LIBs) is usually lower than 250 Wh kg⁻¹ and no longer meets


In the past decade, many strategies have been proposed to solve the crucial problems of Li anode, such as optimizing electrolyte composition,^[12–19] engineering solid-electrolyte/solid interface layers,^[20–24] and modifying the substrate or host structures for Li metal.^[25–31] Among these routes, the construction of Li host structures especially for 3D electrodes has received great interest because it's an effective way to regulate Li deposition, suppress Li dendrites, and reduce the local current density.^[32–34] Besides, the 3D porous host for confined Li deposition can accommodate the large volume changes during electroplating and stripping.^[35] Nevertheless, most of the typical 3D host materials, such as copper and carbon, display poor affinity for lithium metal.^[27–29,36] Another efficient strategy to regulate Li deposition is through controlling heterogeneous nucleation behavior.^[37,38] Cui et al.^[39] reported a nanocapsule structure of lithium metal by inducing Li deposition into the hollow carbon spheres with gold nanoparticles inside. Such nanomaterial has zero overpotential for Li nucleation and could be utilized as seeds for Li selective deposition.

Integrating the above strategies for resolving the fundamental problems of Li anode, herein, we report ultrafine silver-nanocrystals-decorated 3D TiO₂ nanotube arrays as confined space host for lithium metal enabling ultrastable electroplating and stripping performance. First, TiO₂ nanotube arrays exhibit much better lithium affinity compared with copper substrate, leading to improved lithium nucleation overpotential and

Y. Lu, J. Wang, Y. Chen, X. Zheng, Dr. H. Yao, Prof. Z. Hong
Fujian Provincial Key Laboratory of Quantum Manipulation
and New Energy Materials
College of Physics and Energy
Fujian Normal University
Fuzhou 350117, China
E-mail: zshong@fjnu.edu.cn

Y. Lu, Dr. H. Yao
Fujian Provincial Collaborative Innovation Center for Advanced
High-Field Superconducting Materials and Engineering
Fuzhou 350117, China

Prof. S. Mathur, Prof. Z. Hong
Institute of Inorganic Chemistry
University of Cologne
Greinstr. 6, Cologne 50939, Germany

 The ORCID identification number(s) for the author(s) of this article can be found under <https://doi.org/10.1002/adfm.202009605>.

DOI: 10.1002/adfm.202009605

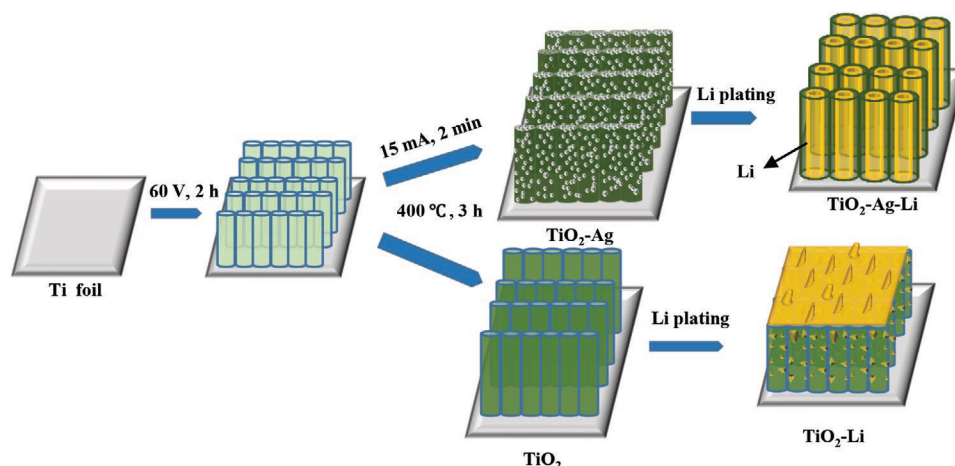


Figure 1. Schematic process of fabricating 3D TNT and TNT-Ag scaffolds and Li deposition on them.

cycling stability. Then, the selective nucleation and deposition of lithium metal into nanotubes were successfully achieved after decorating ultrafine and homogeneous silver nanocrystals acting as nanoseeds. Such 3D electrode of lithium incorporation into 1D nanotube arrays is first obtained enabling effective solving of lithium dendrites and volume change as well as fast electron transport. The 3D TiO_2 nanotube arrays decorated by silver nanocrystals exhibit high Coulomb efficiency, ultralow overpotential, and long-term cycling life over 2500 h with 2 mAh cm^{-2} at a current density of 1 mA cm^{-2} in a $\text{Li} \parallel \text{Li}$ symmetric cell.

2. Results and Discussion

Figure 1 presents the schematic fabrication process of 3D TiO_2 nanotube (TNT) arrays, and then decorated with ultrafine silver nanocrystals (TNT-Ag). First, TNT precursors were prepared by the classical anodic oxidation method, and thus obtaining the crystalline TNT through calcination at $400 \text{ }^\circ\text{C}$. TNT-Ag was prepared by depositing silver nanocrystals on TNT precursors with two-step cathodic reduction method, following heat treatment at the same temperature. Schematic diagram of fabricating TNT-Ag by cathode reduction method is presented in Figure S1, Supporting Information; under the action of an external circuit, Ag^+ gains electrons at the cathode and was reduced, while O^{2-} lost electrons at the opposite electrode to form oxygen. Two-step reduction route was practised and washing with deionized water and alcohol at each step to guarantee that most of the decorated silver was located inside the wall of nanotube. Finally, lithium metal was electrochemically deposited into the TNT and TNT-Ag to make Li composite anode for comparative study.

The XRD patterns of TNT and TNT-Ag are shown in Figure S2a, Supporting Information. It can be seen that both scaffolds obtained after calcination are pure anatase TiO_2 phase (JCPDS: 21-1272). It should be noted that Ag characteristic diffraction peak of TNT-Ag is not found which may be due to the low content or small crystalline size. To further verify the existence and chemical state of silver, XPS analysis was conducted for TNT-Ag, as shown in Figure S2b-d, Supporting

Information. The XPS survey spectrum (Figure S2b, Supporting Information) confirms the presence of only TiO_2 and Ag species in the scaffold. The peak of 368.0 eV in Ag 3d confirms the exclusive existence of metallic silver (Ag^0), while Ti 2p (Figure S2d, Supporting Information) belongs to typical Ti^{4+} . It can be seen from the SEM images that the TiO_2 scaffold is composed of a uniform and highly oriented nanotube array with a diameter $\approx 110 \text{ nm}$ and a length $\approx 8 \text{ } \mu\text{m}$ (Figure 2a,b). As shown in Figure 2c, the edge and inner wall of nanotubes were decorated with uniform silver nanoparticles, as highlighted in the inset. It should be mentioned that the 1D nanotube channel is still in reserve. Fewer silver nanocrystals grew at the outer wall of nanotube due to the limited space (Figure 2d). In order to further investigate the composition of TNT-Ag, the EDX mapping at cross-section is shown in Figure S3, Supporting Information, which verifies the existence of Ag. The content of Ag is around 7% in weight. It's worth mentioning that different deposition manners give rise to a remarkable effect on the result of Ag decoration. As shown from the SEM image in Figure S4, Supporting Information, obtained from direct electrodeposition with constant current of 15 mA for 2 min , a few Ag nanoparticles with relatively large size around 20 nm but less content are found and can't achieve homogeneous decoration. We also found that many white products fall off when the TNT film was taken out. This should be due to the over growth of Ag nanocrystals, and then loss of adherence to the substrate. Combining with the XPS result, chemical adsorption is the main interaction between TiO_2 and Ag particles, only very small Ag nanoparticles with high surface energy can be adsorbed on TNT. Two-step deposition way with only one minute each time effectively guarantees the homogeneous electroplating of ultrafine Ag nanocrystals.

Transmission electron microscopy (TEM) (Figure 2e) further reveals the spatial distribution of silver nanoparticles; many of them are located inside the nanotube. HRTEM image (Figure 2f) shows that lattice fringes with interspacing of 0.36 nm can be assigned to the (101) plane of anatase TiO_2 . It is interesting that the lattice fringes of the silver nanoparticles with diameter $7\text{--}10 \text{ nm}$ are almost invisible because they are located on the inner wall of the nanotube. Indeed, the silver

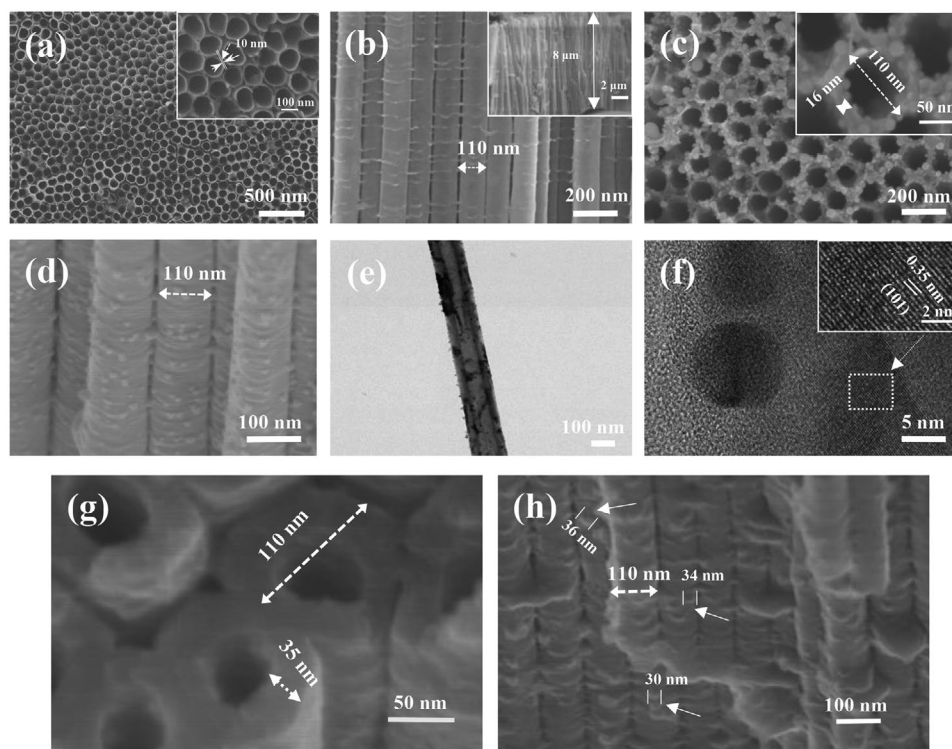


Figure 2. SEM images of a,b) TNT and c,d) TNT-Ag. e) TEM and f) HRTEM images of TNT-Ag. g,h) SEM images of Li nucleation on TNT-Ag with a plating capacity of 0.5 mA h cm^{-2} .

nanoparticles outside the nanotube display clear lattice fringes with interspacing of 0.21 nm (Figure S5, Supporting Information). It's found that silver nanoparticles on the inner wall of the nanotube are especially crucial for inducing lithium metal deposition inside the nanotubes. In order to investigate the effect of 3D TNT-Ag on the inhibition of lithium dendrite, we studied the nucleation of Li metal on TNT-Ag and TNT matrix by electroplating lithium metal. The electrodes are all activated for 5 cycles. After the deposition of lithium metal with 0.5 mA h cm^{-2} at a current density of 1 mA cm^{-2} , the thickness of TNT film increased from initial 8 to $13 \mu\text{m}$ (Figure S6a, Supporting Information); the nanotube channel of TNT is blocked and dendritic lithium metals grew on the top surface of the nanotube (Figure S6b, Supporting Information). Under depositing 1 mA h cm^{-2} (Figure S6c, Supporting Information), the electrode thickness remarkably increased to $25 \mu\text{m}$. The blocking of channel and uneven Li growth are also found in closed TNT scaffold-based Li anode which was made by the infiltration of molten Li metal into the channel.^[31] Thus, they fabricated spaced or loose TiO_2 nanotubes to improve the Li metal blocking on the film surface during Li infiltration process. However, such TNT can't afford high loading mass of Li metal due to the too small film thickness around $1 \mu\text{m}$. As for TNT-Ag, as shown in Figure 2g, we can see that the shape of the nanotube arrays remains intact after lithium metal deposition. Interestingly, the channel of nanotubes is not blocked by lithium metal, leading to the formation of 1D and dendrite-free lithium metal nanocapsules. At the same time, the nanotubes wall after lithium metal deposition increased from 16 to 35 nm , and the diameter is still around 110 nm (Figure 2g), suggesting

lithium metal electroplated into the inside wall of nanotube after silver decoration, which effectively restrains the sedimentary formation of lithium metal on the top surface and the growth of lithium dendrite. From SEM image of section view (Figure 2h), it's further observed that a few lithium metals electroplated on the outside wall of nanotube from the nearly constant external diameter. Nevertheless, we can see the Li preferred deposition on Ag nanoparticles ($9\text{--}15 \text{ nm}$ in Figure 2d) from the increased diameter to $33\text{--}37 \text{ nm}$. When the plating capacity increases to 1 mA h cm^{-2} on TNT-Ag, additional Li nucleation and deposition was performed on the surface of nanotube array (Figure S6d,e, Supporting Information). Nevertheless, it's remarkably shown that a smooth lithium deposition without any whisker lithium is found. The compact Li metal deposition is achieved from the much lower electrode thickness, $14 \mu\text{m}$ for TNT-Ag versus $25 \mu\text{m}$ for TNT. It's suggested that the smooth and uniform epitaxial deposition of lithium metal anode is enabled by the little nucleation barrier on the substrate at the initial stage. This will be further discussed below from the view of ultralow overpotential for Li nuclei deposited on TNT-Ag.

Cyclic voltammetry (CV) (Figure S7a, Supporting Information) method was adopted to study the electrochemical behavior of TNT-Ag. A cathodic peak around 1.4 V at the first cycle is observed, which could be due to the insertion of lithium-ion into TiO_2 . A pair redox peak between -0.2 and 0.3 V is clearly shown, corresponding to the electroplating/stripping of Li metal. Figure 3a shows galvanostatic voltage profiles of Li plating/stripping on Cu, TNT, and TNT-Ag substrates performed with a capacity of 0.5 mA h cm^{-2} at a current density of 1 mA cm^{-2} . For Cu substrate, its nucleation overpotential

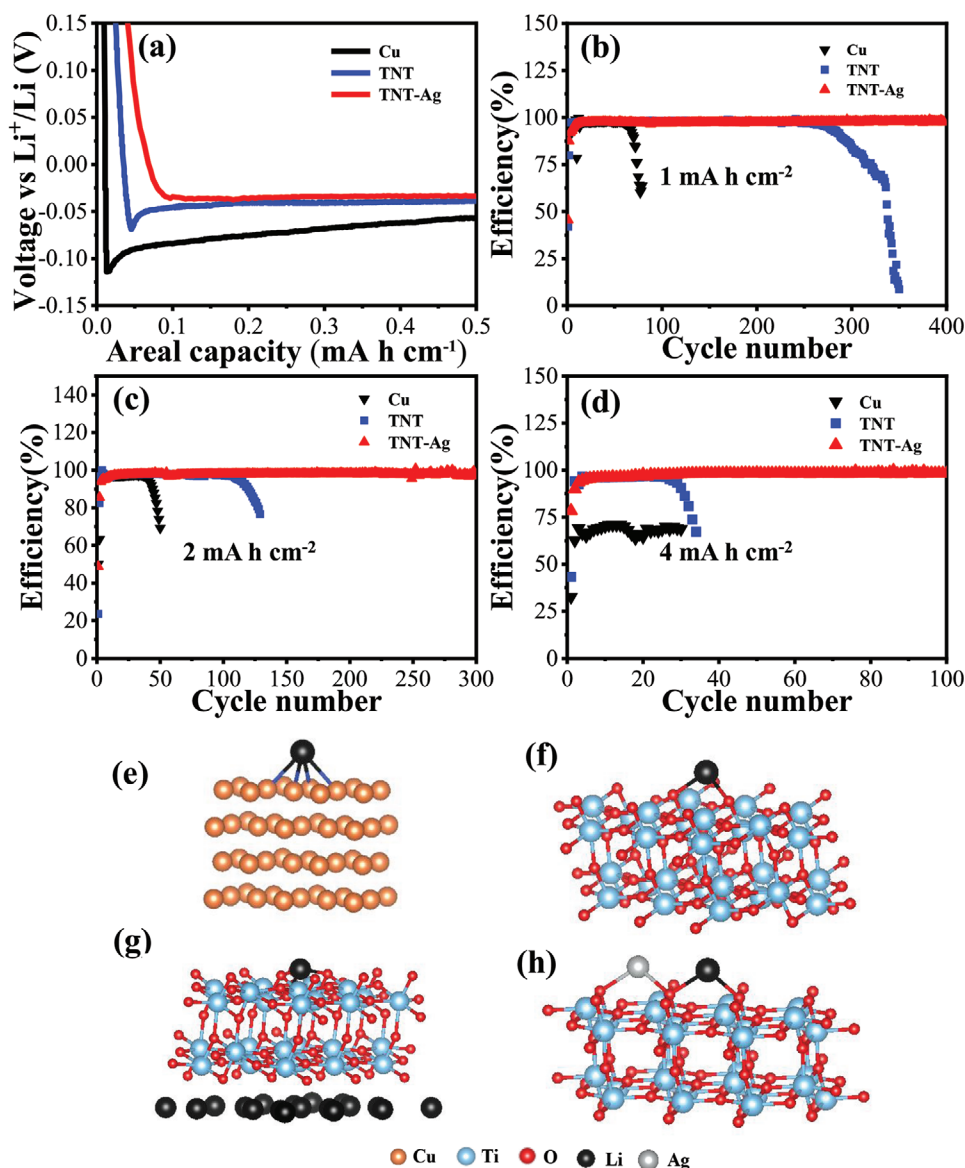


Figure 3. a) Galvanostatic voltage profiles of Li plating on Cu, TNA, and TNA-Ag substrates performed with a capacity of 0.5 mA h cm^{-2} at a current density of 1 mA cm^{-2} . Coulombic efficiency of Li anode on the three substrates with a capacity of b) 1 mA h cm^{-2} , c) 2 mA h cm^{-2} , and d) 4 mA h cm^{-2} under 1 mA cm^{-2} . The most stable adsorption configurations of Li on the structure of e) Cu, f) TiO_2 , g) $\text{Li}_{0.5}\text{TiO}_2$, and h) $\text{TiO}_2\text{-Ag}$.

at 1 mA cm^{-2} reaches up to 64 mV, but it reduces to 35 mV for TNT. This result clearly indicates the better lithiophilic property of TNT than copper substrate, which is necessary and favorable for homogeneous Li deposition. Moreover, TNT-Ag provides a lowest nucleation overpotential near 0 mV, which is also found for the Au or Ag substrate.^[39] This is essential for the spatial control of Li deposition site. Thanks to no nucleation barriers of Li deposition on Ag, Li metal electroplating occurs in the inside wall of nanotube facilitating the formation of 1D lithium metal nanocapsules (Figure 2g). It's found that Ag content plays important role on the nucleation overpotential. As shown in Figure S8, Supporting Information, there still exists the nucleation overpotential around 13 mV of TNT-Ag with low Ag content (2.6%) obtained under 1 min electroplating.

Figure 3b shows the cycling Coulombic efficiency of Li anode on the three substrates with 1 mA h cm^{-2} at 1 mA cm^{-2} . It's found that the Coulombic efficiency drops quickly for Cu substrate after 50 cycles, while it can maintain around 98.5% for TNT after 250 cycles and then decays. A high Coulombic efficiency about 99.3% can be maintained even after 400 cycles for TNT-Ag, indicating excellent cycling performance. Under higher plating capacity of 2 mA h cm^{-2} (Figure 3c) and 4 mA h cm^{-2} (Figure 3d), the Coulombic efficiency of Cu and TNT substrates drops quickly with the increasing cycling. While a high Coulombic efficiency around 99.4% can be maintained for TNT-Ag even after 300 cycles with 2 mA h cm^{-2} and 100 cycles with 4 mA h cm^{-2} . In addition, it's worth mentioning that the small inner diameter of nanotubes also facilitates the stable lithium deposition. As shown in Figure S9, Supporting

Information, the Coulombic efficiency for TNT-45 V with larger inner diameter ≈ 25 nm will gradually drop after 80 cycles. This is because TNT with small inner diameter owning larger surface area could be favorable for reducing the local electroplating current density and provides larger space for lithium deposition.

Density functional theory (DFT) calculations were performed to illustrate the intrinsic Li deposition behavior on different substrate. Generally, Li absorption energy on the substrate should be larger than the Li cohesive in order to avoid the formation of Li bulk. As shown in Figure 3e–g, the Li absorption energy on the surface of Cu, TiO_2 , and $\text{Li}_{0.5}\text{TiO}_2$ were calculated to be -0.41 , -2.00 , and -1.97 eV, respectively. $\text{Li}_{0.5}\text{TiO}_2$ is also considered because the lithiation occurred during the first cycle for anatase TiO_2 as revealed in the CV curves. This suggests that both TiO_2 and $\text{Li}_{0.5}\text{TiO}_2$ exhibit much larger absorption energy compared with Cu substrate, which is favorable for stable and uniform Li deposition. Nevertheless, pristine TiO_2 still has an unavoidable overpotential (35 mV) which may be due to its remarkably different crystal structure with Li. Ag decoration in nanoscale effectively solves this issue benefiting from the high solubility and compatibility with Li. Cui et al. also demonstrated that the low overpotential generated little number of nuclei in the instantaneous nucleation, which can be used to improve the uniformity of deposited Li metal.^[40] Herein, we also discuss it in view of DFT calculation. The adsorption configuration of Li on TiO_2 -Ag is presented in Figure 3h. The calculated Li absorption energy on the surface of TiO_2 -Ag is -1.71 eV. This is much larger absorption energy compared with Cu substrate, providing enough strong energy for Li capture. Moreover, this value suggests that the presence of Ag can decrease the over large Li absorption energy on the surface of TiO_2 (-2.00 eV). This may be favorable for the easy Li desorption on TiO_2 scaffold and avoid the Li loss, leading to improved Coulombic efficiency.

EIS spectra and their fitting (Figure S7b,c, Supporting Information) reveal the electrochemically improved process of TNT-Ag during cycling. In the initial state, the interface charge transfer resistance for TNT-Ag is about 32Ω for TNT which is smaller than TNT (45Ω), indicating the better electronic transport after Ag decoration. The resistance decreased to 14 and 6Ω after 100 cycles for TNT and TNT-Ag respectively, which is consistent with the continuous increasing Coulomb efficiency in the first 100 cycles. However, after 200 cycles, the resistance of TNT quickly increased over 62Ω , while TNT-Ag is still less than the initial state. This result verifies the improved electronic transport for TNT-Ag at the electrode interface through inhibiting the formation of thick SEI layer which facilitates the rate capability. Besides, the interface electric-field effect existing in binary composite structure may facilitate the charge transfer dynamics, as illustrated in previous reports.^[41–43] Moreover, it's deduced that the Li-ion diffusion coefficients in the TNT-Ag-Li and TNT-Li anodes after 200 cycles are 6.6×10^{-10} and $3.8 \times 10^{-10} \text{ cm}^2 \text{ s}^{-1}$, respectively. The improved Li-ion diffusion performance may be due to the smooth Li plating after Ag decoration and well remained 3D channel during cycling.

The Li || Li symmetric cell tests were used to evaluate the interfacial stability of Li metal anodes upon repeated

Li plating/stripping processes. Figure 4a shows the T - V curve of lithium deposition at 2 mA h cm^{-2} at 1 mA cm^{-2} . The voltage overpotential of TNT anode is about 14 mV at the beginning, then increases and fluctuates drastically with the increasing cycles within working for 400 h. In contrast, as highlighted in the enlarged figure, TNT-Ag anode displays an ultrasmall overpotential of less than 4 mV, which could be very stable even after cycling for 2500 h without any apparent increase of voltage hysteresis. Overpotential or polarization voltage for electrode generally comes from concentration polarization voltage and electrochemical polarization voltage, which arises from overdue ions diffusion and extra electronics accumulation without complete transfer respectively. Such ultrasmall overpotential presented in this work illustrates the exceptional ions diffusion performance and outstanding reaction kinetics for TNT-Ag composite Li anode. In order to test the stability of lithium metal deposition with large capacity, we tested the electrode deposited lithium metal with 4 mA h cm^{-2} , as shown in Figure 4b. The voltage overpotential is about 58 mV for TNT anode and the working voltage fluctuates seriously which could only be maintained for 110 h. While for TNT-Ag anode, the voltage overpotential is only around 12 mV and keeps stable up to 1400 h. In a word, to the best of our knowledge, this is the minimum overpotential up to now among various substrates and one of the best Li metal anodes as highlighted in the Table S1, Supporting Information. Besides, as presented in Figure S10, Supporting Information, TNT-Ag-Li exhibits excellent rate capability from 0.5 to 10 mA cm^{-2} with a capacity of 2 mA h cm^{-2} . As discussed in the morphology formation of Li anode, uneven lithium dendrites and thick SEI layer will occur on the surface of TNT electrode with the increasing cycles, which would lead to the rise of the charge transfer resistance and voltage overpotential. In contrast, the ultrasmall overpotential and excellent cycling stability of TNT-Ag is attributed to the confined space Li deposition enabled by the ultrafine and homogeneous silver decorating which possesses zero nucleation barrier. Although 3D nanotube array has been reported as scaffold for Li metal through Li melt diffusion into space between nanotubes, the present study is the first achievement in confined space Li deposition inside the nanotubes. As a result, this result also demonstrates the outstanding performance of real 1D composite Li metal anode.

To demonstrate the feasibility of such a design in practical application, we assembled bare Li metal and Li-plated TNT, TNT-Ag anodes with commercial LiFePO_4 (LFP) cathode for investigating the application potential in full cells. The structure and morphology characterization are shown in Figure S11, Supporting Information, which determines the pure phase LiFePO_4 with size of 200–500 nm. It can be seen from Figure 5a that LFP || TNT-Ag-Li displays the highest discharge capacity. The initial Coulombic efficiency of LFP||Li and LFP||TNT-Li is 90% and 95%, suggesting the improved reversibility of Li-ion on 3D TNT scaffold. Remarkably, we carried out a full cell test for TNT-Ag-Li under 5 C current density (Figure 5d). It has surprisingly excellent performance at high current density. After 500 cycles, it still has a specific capacity of 110 mA h g^{-1} with

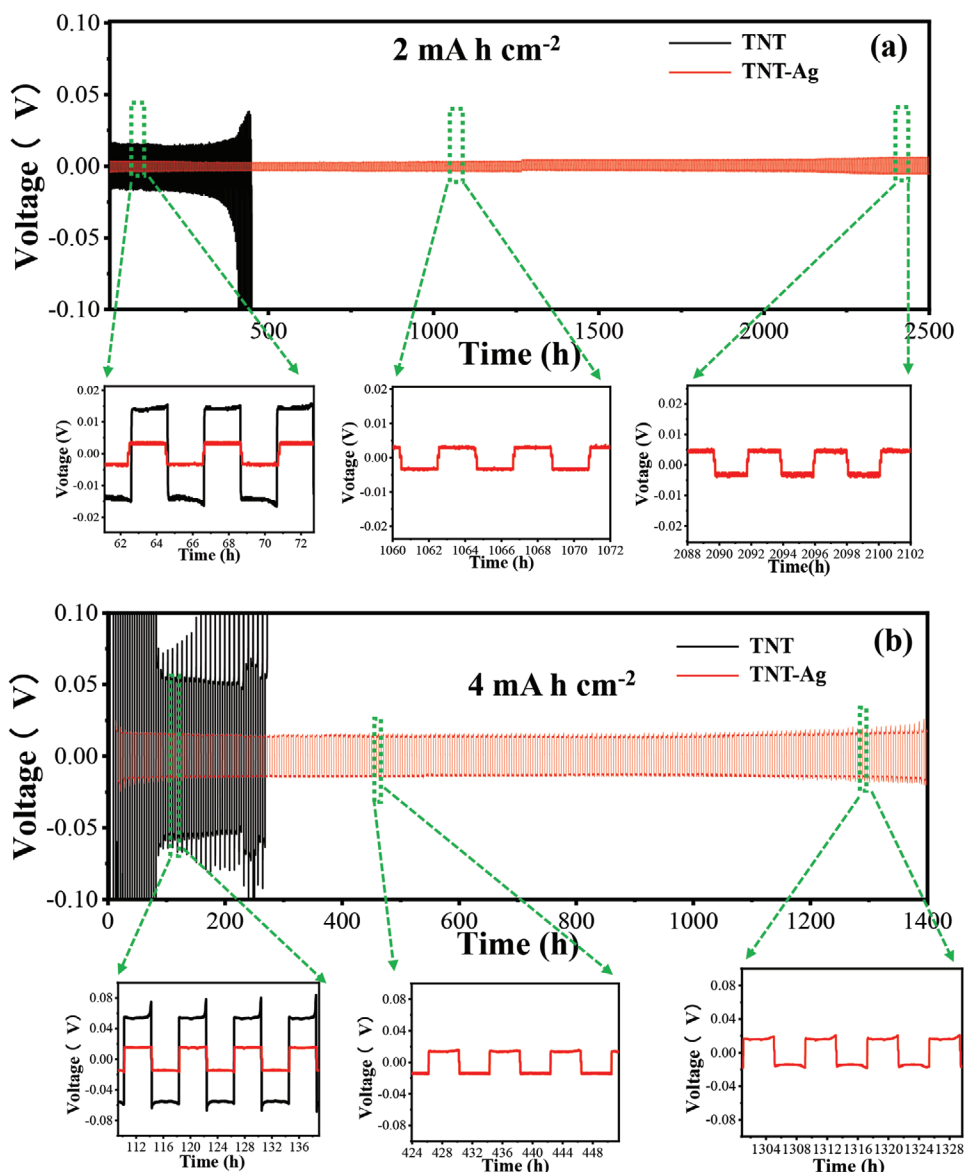


Figure 4. Voltage profiles of metallic Li plating/stripping on TNT and TNT-Ag substrates at 1 mA cm^{-2} with capacity of a) 2 mA h cm^{-2} and b) 4 mA h cm^{-2} and their corresponding enlarged figures at selective areas.

a capacity retention up to 96%, and high Coulomb efficiency around 100%.

3. Conclusions

In summary, ultrafine silver-nanocrystals-decorated 3D TiO_2 nanotube arrays were first fabricated and used as a confined space for lithium deposition, demonstrating ultrastable lithium metal electroplating and stripping performance. Such binary structure addresses the essential requirements for regulating uniform lithium deposition. TiO_2 material possesses superior lithium affinity, ultrafine silver nanocrystals decoration provides the selective and uniform nucleation in nanoscale without overpotential, 1D nanotube arrays effectively accommodate

volume change of lithium anode and facilitate fast ions and electrons transport. Finally, lithium anode hosted in such scaffold displays high Coulomb efficiency, ultralow overpotential, and long-term cycling life.

4. Experimental Section

Material Synthesis: TiO_2 nanotube arrays (TNT) precursor was fabricated by typical anodic oxidation process. First, the titanium sheet (99.99%, 0.1 mm) was cut into the size of $1.2 \text{ cm} \times 1.2 \text{ cm}$ and sanded, and then placed in acetone, ethanol, and deionized water with ultrasonic cleaning for 30 min, respectively. Second, the electrolyte was prepared by mass ratio of 0.25% NH_4F , 0.75% deionized water, and 99% ethylene glycol. Finally, TNT was prepared by electrolysis at 60 V constant voltage for 1 h at a constant temperature of $25 \text{ }^\circ\text{C}$ with the

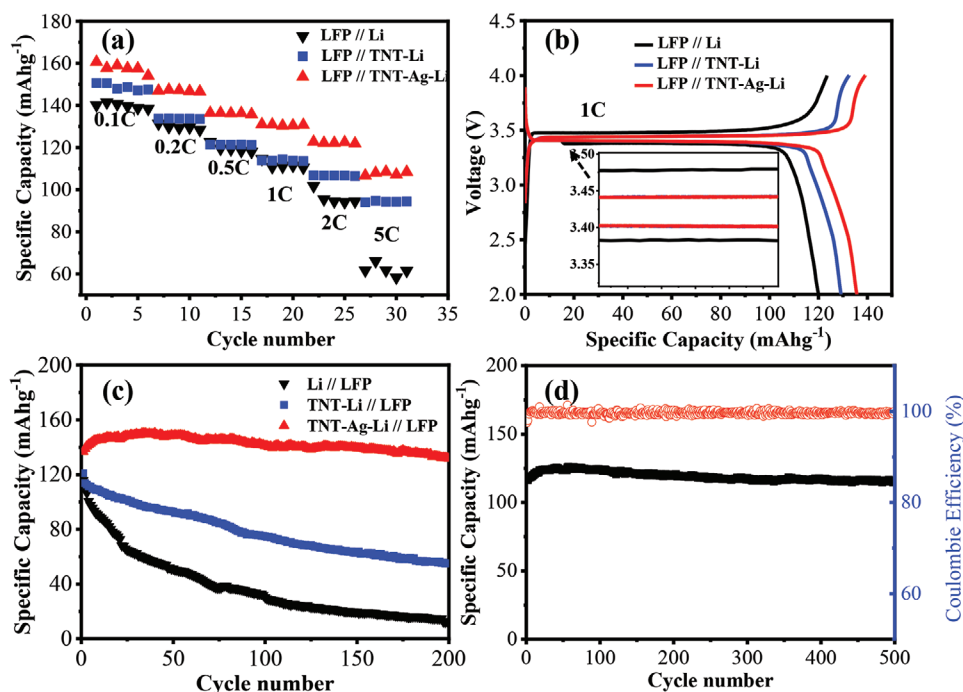


Figure 5. Electrochemical performance of different batteries constructed by LFP // Li, LFP // TNT-Li and LFP // TNT-Ag-Li: a) Rate capability at various rates from 0.1 to 5 C, b) charge/discharge profiles at 1C, c) cycling stability at 1C and d) 5C.

treated titanium sheet as anode and Pt network as cathode. In order to investigate the effect of diameter upon Li deposition, TNT-45 V sample with small inner diameter of nanotube was also prepared under the constant electrolysis voltage at 45 V. TNT-Ag was prepared by depositing silver nanocrystals on TNT precursors with cathodic reduction method with TNT precursor as cathode, Pt network as anode, and 0.1 M AgNO_3 (ethylene glycol solution) as electrolyte, following heat treatment at 400 °C for 3 h in Ar atmosphere. In order to obtain the homogenous decoration with ultrafine silver nanocrystals, two step electrodeposition process with 15 mA constant current for 1 min in each time, and the surface of the electrode was washed with deionized water and alcohol.

Supporting Information

Supporting Information is available from the Wiley Online Library or from the author.

Acknowledgements

Y.L. and J.W. contributed equally to this work. This work was financially supported by National Natural Science Foundation of China (NSFC 51874099 and 21805038) and National Science Foundation of Fujian Province (2018J06012). Z.H. is thankful for the support from Alexander von Humboldt-Stiftung/Foundation. The authors are also thankful for the Undergraduate Training Programs for Innovation and Entrepreneurship of Fujian Normal University (S202010394018).

Conflict of Interest

The authors declare no conflict of interest.

Keywords

host, lithium metal anodes, silver nanocrystals decoration, TiO_2 nanotubes

Received: November 10, 2020

Revised: December 7, 2020

Published online:

- [1] M. Armand, J.-M. Tarascon, *Nature* **2008**, 451, 652.
- [2] R. V. Noorden, *Nature* **2014**, 507, 26.
- [3] T. Placke, R. Kloepsch, S. Dühnen, M. Winter, *J. Solid State Electrochem.* **2017**, 21, 1939.
- [4] D. Lin, Y. Liu, Y. Cui, *Nat. Nanotechnol.* **2017**, 12, 194.
- [5] T. Tao, S. Lu, Y. Fan, W. Lei, S. Huang, Y. Chen, *Adv. Mater.* **2017**, 29, 201700542.
- [6] J. Xu, J. Ma, Q. Fan, S. Guo, S. Dou, *Adv. Mater.* **2017**, 29, 201606454.
- [7] P. Albertus, S. Babinec, S. Litzelman, A. Newman, *Nat. Energy* **2017**, 3, 16.
- [8] J. Liu, Z. Bao, Y. Cui, E. J. Dufek, J. B. Goodenough, P. Khalifah, Q. Li, B. Y. Liaw, P. Liu, A. Manthiram, Y. S. Meng, V. R. Subramanian, M. F. Toney, V. V. Viswanathan, M. S. Whittingham, J. Xiao, W. Xu, J. Yang, X.-Q. Yang, J.-G. Zhang, *Nat. Energy* **2019**, 4, 180.
- [9] S. Tang, Y. Y. Zhang, X. G. Zhang, J. T. Li, X. Y. Wang, J. W. Yan, D. Y. Wu, M. S. Zheng, Q. F. Dong, B. W. Mao, *Adv. Mater.* **2019**, 31, 1807495.
- [10] B. Wu, J. Lochala, T. Taverne, J. Xiao, *Nano Energy* **2017**, 40, 34.
- [11] Y. Li, Y. Li, A. Pei, K. Yan, Y. Sun, C.-L. Wu, L.-M. Joubert, R. Chin, A. L. Koh, Y. Yu, J. Perrino, B. Butz, S. Chu, Y. Cui, *Science* **2017**, 358, 506.
- [12] S. Li, M. Jiang, Y. Xie, H. Xu, J. Jia, J. Li, *Adv. Mater.* **2018**, 30, 1706375.
- [13] N. Piao, X. Ji, H. Xu, X. Fan, L. Chen, S. Liu, M. N. Garaga, S. G. Greenbaum, L. Wang, C. Wang, X. He, *Adv. Energy Mater.* **2020**, 10, 1903568.

- [14] Z. Wang, F. Qi, L. Yin, Y. Shi, C. Sun, B. An, H. M. Cheng, F. Li, *Adv. Energy Mater.* **2020**, *10*, 1903843.
- [15] Z. Zeng, V. Murugesan, K. S. Han, X. Jiang, Y. Cao, L. Xiao, X. Ai, H. Yang, J.-G. Zhang, M. L. Sushko, J. Liu, *Nat. Energy* **2018**, *3*, 674.
- [16] Y. Lu, K. Korf, Y. Kambe, Z. Tu, L. A. Archer, *Angew. Chem., Int. Ed.* **2014**, *53*, 488.
- [17] X. Fan, L. Chen, O. Borodin, X. Ji, J. Chen, S. Hou, T. Deng, J. Zheng, C. Yang, S. C. Liou, K. Amine, K. Xu, C. Wang, *Nat. Nanotechnol.* **2018**, *13*, 715.
- [18] S. Choudhury, L. A. Archer, *Adv. Electron. Mater.* **2016**, *2*, 1500246.
- [19] M. D. Tikekar, S. Choudhury, Z. Tu, L. A. Archer, *Nat. Energy* **2016**, *1*, 16114.
- [20] X. Han, Y. Gong, K. K. Fu, X. He, G. T. Hitz, J. Dai, A. Pearse, B. Liu, H. Wang, G. Rubloff, Y. Mo, V. Thangadurai, E. D. Wachsman, L. Hu, *Nat. Mater.* **2017**, *16*, 572.
- [21] K. Nie, Y. Hong, J. Qiu, Q. Li, X. Yu, H. Li, L. Chen, *Front. Chem.* **2018**, *6*, 616.
- [22] Z. Shen, W. Zhang, G. Zhu, Y. Huang, Q. Feng, Y. Lu, *Small Methods* **2019**, *4*, 1900592.
- [23] S. Wenzel, S. J. Sedlmaier, C. Dietrich, W. G. Zeier, J. Janek, *Solid State Ionics* **2018**, *318*, 102.
- [24] K. Liu, A. Pei, H. R. Lee, B. Kong, N. Liu, D. Lin, Y. Liu, C. Liu, P. C. Hsu, Z. Bao, Y. Cui, *J. Am. Chem. Soc.* **2017**, *139*, 4815.
- [25] P. Shi, X. Q. Zhang, X. Shen, R. Zhang, H. Liu, Q. Zhang, *Adv. Mater. Technol.* **2019**, *5*, 1900806.
- [26] W. Xu, J. Wang, F. Ding, X. Chen, E. Nasybulin, Y. Zhang, J.-G. Zhang, *Energy Environ. Sci.* **2014**, *7*, 513.
- [27] H. Ye, S. Xin, Y. X. Yin, J. Y. Li, Y. G. Guo, L. J. Wan, *J. Am. Chem. Soc.* **2017**, *139*, 5916.
- [28] Z. Lu, S. Liu, C. Li, J. Huang, D. Wu, R. Fu, *Chem. Commun.* **2019**, *55*, 6034.
- [29] Y. Shi, Z. Wang, H. Gao, J. Niu, W. Ma, J. Qin, Z. Peng, Z. Zhang, *J. Mater. Chem. A* **2019**, *7*, 1092.
- [30] S. Wu, Z. Zhang, M. Lan, S. Yang, J. Cheng, J. Cai, J. Shen, Y. Zhu, K. Zhang, W. Zhang, *Adv. Mater.* **2018**, *30*, 201705830.
- [31] K. Tantratian, D. Cao, A. Abdelaziz, X. Sun, J. Sheng, A. Natan, L. Chen, H. Zhu, *Adv. Energy Mater.* **2019**, *10*, 1902819.
- [32] Y. Xia, Y. Jiang, Y. Jiang, W. Zhang, Y. Wang, S. Wang, Y. Liu, W. Sun, X.-Z. Zhao, *J. Power Sources* **2019**, *442*, 227214.
- [33] C. Jin, O. Sheng, J. Luo, H. Yuan, C. Fang, W. Zhang, H. Huang, Y. Gan, Y. Xia, C. Liang, J. Zhang, X. Tao, *Nano Energy* **2017**, *37*, 177.
- [34] H. Wang, J. Wu, L. Yuan, Z. Li, Y. Huang, *ACS Appl. Mater. Interfaces* **2020**, *12*, 28337.
- [35] P. Yao, Q. Chen, Y. Mu, J. Liang, X. Li, X. Liu, Y. Wang, B. Zhu, J. Zhu, *Mater. Chem. Front.* **2019**, *3*, 339.
- [36] Q. Li, S. Zhu, Y. Lu, *Adv. Funct. Mater.* **2017**, *27*, 1606422.
- [37] X. Chen, X.-R. Chen, T.-Z. Hou, B.-Q. Li, X.-B. Cheng, R. Zhang, Q. Zhang, *Sci. Adv.* **2019**, *5*, eaau7728.
- [38] P. Xue, S. Liu, X. Shi, C. Sun, C. Lai, Y. Zhou, D. Sui, Y. Chen, J. Liang, *Adv. Mater.* **2018**, *30*, 1804165.
- [39] K. Yan, Z. Lu, H.-W. Lee, F. Xiong, P.-C. Hsu, Y. Li, J. Zhao, S. Chu, Y. Cui, *Nat. Energy* **2016**, *1*, 16010.
- [40] A. Pei, G. Zheng, F. Shi, Y. Li, Y. Cui, *Nano Lett.* **2017**, *17*, 1132.
- [41] T. Meng, B. Li, Q. Wang, J. Hao, B. Huang, F. L. Gu, H. Xu, P. Liu, Y. Tong, *ACS Nano* **2020**, *14*, 7066.
- [42] T. Meng, B. Li, L. Hu, H. Yang, W. Fan, S. Zhang, P. Liu, M. Li, F. L. Gu, Y. Tong, *Small Methods* **2019**, *3*, 1900185.
- [43] Y. Huang, Z. Guo, H. Liu, S. Zhang, P. Wang, J. Lu, Y. Tong, *Adv. Funct. Mater.* **2019**, *29*, 1903490.